

Beyond Score Changes: Adversarial Attack on No-Reference Image Quality Assessment from Two Perspectives

Chenxi Yang
NERCVT, School of Mathematical
Sciences, Peking University
Beijing, China
yangchenxi@stu.pku.edu.cn

Yujia Liu
NERCVT, School of Computer
Science, Peking University
Beijing, China
yujia_liu@pku.edu.cn

Dingquan Li
Peng Cheng Laboratory
Shenzhen, China
dingquanli@pku.edu.cn

Yan Zhong
NERCVT, School of Mathematical
Sciences, Peking University
Beijing, China
zhongyan@stu.pku.edu.cn

Tingting Jiang✉
NERCVT, School of Computer
Science, Peking University
Beijing, China
ttjiang@pku.edu.cn

ABSTRACT

Deep neural networks have demonstrated impressive success in No-Reference Image Quality Assessment (NR-IQA). However, recent researches highlight the vulnerability of NR-IQA models to subtle adversarial perturbations, leading to inconsistencies between model predictions and subjective ratings. Current adversarial attacks, however, focus on perturbing predicted scores of individual images, neglecting the crucial aspect of inter-score correlation relationships within an entire image set. Meanwhile, it is important to note that the correlation, like ranking correlation, plays a significant role in NR-IQA tasks. To comprehensively explore the robustness of NR-IQA models, we introduce a new framework of **correlation-error-based attacks** that perturb both the correlation within an image set and score changes on individual images. Our research primarily focuses on ranking-related correlation metrics like Spearman’s Rank-Order Correlation Coefficient (SROCC) and prediction error-related metrics like Mean Squared Error (MSE). As an instantiation, we propose a practical two-stage **SROCC-MSE-Attack (SMA)** that initially optimizes target attack scores for the entire image set and then generates adversarial examples guided by these scores. Experimental results demonstrate that our SMA method not only significantly disrupts the SROCC to negative values but also maintains a considerable change in the scores of individual images. Meanwhile, it exhibits state-of-the-art performance across metrics with different categories. Our method provides a new perspective on the robustness of NR-IQA models.

1 INTRODUCTION

Deep Neural Networks (DNNs) have demonstrated impressive capabilities in diverse domains, as exemplified by their outstanding performance in a range of studies [5, 9, 38]. Among these, Image Quality Assessment (IQA) stands out as a noteworthy application [16, 19, 38, 43]. The primary objective of IQA is to predict quality scores for input images, aligning with Mean Opinion Scores (MOS) derived from subjective studies, which provide facilities for the evaluation of multimedia tasks [18, 44]. IQA models can be categorized into Full-Reference (FR) and No-Reference (NR) types based on the availability of reference images: FR-IQA models have access to the reference image, while NR-IQA models do not [3, 6].

NR-IQA is crucial for designing and optimizing real-world image processing algorithms where the reference image is unavailable, and its growing popularity is attributed to its broader applicability compared to FR-IQA. The evaluation of NR-IQA models is conducted using two major categories of metrics. The first category comprises **error-based** metrics that measure the prediction error for a single image, such as Mean Squared Error (MSE) and Mean Absolute Error (MAE). The second category is **correlation-based**, it calculates the correlation relationship between the predicted scores and MOS of a set of images, as observed in metrics like Spearman’s Rank Order Correlation Coefficient (SROCC) [33], Kendall Rank Order Correlation Coefficient (KROCC) [13], and Pearson Linear Correlation Coefficient (PLCC) [23].

Despite these advances, recent research has unveiled a critical issue – the vulnerability of NR-IQA models to adversarial attacks [1, 21, 37, 41]. These attacks added subtle perturbations to input images, thus leading to errors in predicted scores while maintaining the appearance of the perturbed image indistinguishable from the original. We refer to such attacks as **error-based attacks**. For instance, Zhang *et al.* [39] perturbed low/high-quality images to yield high/low predicted scores, which resulted in a significant Root Mean Squared Error (RMSE) between predicted scores before and after the attacks. Besides, some research has concentrated on the score changes across a set of images. Shumitskaya *et al.* [28] devised a universal perturbation trained for a given set of images to increase their predicted scores.

While error-based attacks effectively underscore the vulnerability of NR-IQA models in the variation of the predicted score, these attacks overlook the impact on correlation-based metrics. As Fig. 1 (left) shows, error-based attacks may randomly increase 10 to 20 points (total 100) to the predicted score of each sample, resulting in a substantial change in predicted scores, but do not significantly alter the relative ranking of these scores. Consequently, such attacks might be ineffective against correlation-based metrics like SROCC. Merely targeting the error-based metrics of NR-IQA models is insufficient for a comprehensive attack strategy. An effective attack should take into account all evaluation metrics of the model, including both error-based metrics and correlation-based metrics. Furthermore, it is important to note that the NR-IQA task is a regression problem where the correlation, like ranking correlation, plays a significant

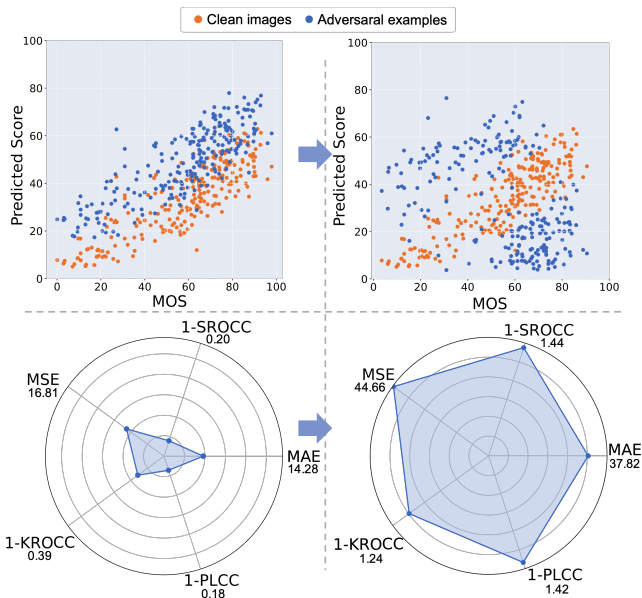


Figure 1: Comparison between error-based attacks (left) and the proposed correlation-error-based attack (right). The first row illustrates the distribution of original scores for clean images and the predicted scores for adversarial examples. Radar charts in the second row assess the attack’s performance across five metrics, with each metric calculated between MOS and predicted scores after the attack. A larger polygon area in the radar charts indicates a better overall performance of the attack method.

role in its applications. This is particularly evident in applications such as image retrieval [17, 32]. Perturbations that affect ranking could seriously compromise retrieval accuracy, underscoring the need to analyze model robustness from the viewpoint of ranking correlation. In light of these insights, considering attacks that disrupt both error-based and correlation-based metrics becomes a pressing need.

To the best of our knowledge, no existing attack frameworks have specifically addressed the disruption of correlation-based metrics, let alone simultaneously tackled both error-based and correlation-based metrics. In this paper, to fill this gap, we propose the framework of **correlation-error-based attacks** for the first time, which demonstrates that attacks of NR-IQA models can effectively impact both error-based and correlation-based metrics concurrently. In this framework, attacks are strategically designed to perturb correlation-based metrics across the entire image set while significantly perturbing the scores for individual samples, as illustrated in Fig. 1 (right). To achieve these goals, we formulate it as a multi-objective optimization problem from both correlation and error perspectives. For the attack objective, we select MSE and SROCC as the two primary objectives in our multi-objective optimization problem. This selection is based on our observation that different error-based metrics exhibit strong positive correlations, which is similar to correlation-based metrics. Therefore, optimizing MSE and SROCC is expected to bring improvements in other related metrics.

After the problem formulation, We consider how to solve this problem. Directly optimizing MSE and SROCC on the whole image set is challenging due to its high dimensionality. Instead of it, we propose a two-stage **SROCC-MSE Attack (SMA)** to generate adversarial examples. In Stage One, our objective is to identify optimal target scores that significantly reduce SROCC and increase MSE between the predicted scores of attacked and clean images. As SROCC is non-differentiable due to the discrete rank function, we approximate it using a differential function and employ the Lagrangian multiplier method to solve the optimization problem. In Stage Two, we utilize the fast gradient sign method [11] to generate adversarial examples, striving to make their predicted scores as close as possible to the target scores identified in Stage One. While exact equivalence between the predicted and target scores may not be achievable, our experiments provide compelling evidence that the discrepancy between them is small.

We conduct experiments on the CLIVE dataset [10], which includes authentic distorted images sourced from the wild and is challenging for NR-IQA. Attacks are conducted on four widely-used NR-IQA models, DBCNN [42], HyperIQA [34], MANIQA [38], and LIQE [43]. Our approach is compared with four existing attack methods, P-attack [41], OUAP [27], K-attack [15], and UAP [28]. Our evaluations spanned seven metrics, considering both error and correlation perspectives. The results demonstrate that SMA offers a powerful attack that influences not only the prediction score of individual images but also the correlation within the set of predicted scores. For instance, in all attacked models, SMA significantly disrupts the SROCC to negative values while simultaneously maintaining a substantial change in the scores of individual images. It demonstrates the effectiveness of SMA within our correlation-error-based attacks framework. The findings underscore the vulnerability of NR-IQA in maintaining individual scores and correlations, paving the way for further research on developing more secure and robust NR-IQA models.

To conclude, the contributions of this paper are:

- This is the first work to propose the correlation-error-based attack framework, which focuses on both score changes in individual images and the correlation within an image set, filling a gap in the field of attacking correlation-based metrics.
- We propose a two-stage SMA method. The Lagrangian multiplier is leveraged to optimize target scores by maximizing score changes (measured by MSE) and disturbing correlation relationships (measured by SROCC). Then individual adversarial images are generated towards target scores.
- Extensive experiments on four NR-IQA models show the superior performance of SMA in attacking both correlation-based metrics and error-based metrics. It offers a novel perspective on attacks on NR-IQA models, contributing to a more comprehensive attack on NR-IQA models.

2 RELATED WORK

In this section, we will introduce existing attack methods on NR-IQA models in Sec. 2.1. As a necessary theoretical basis for optimizing ranking property, the differential ranking methods are introduced in Sec. 2.2.

2.1 Attacks on NR-IQA Models

Existing attacks on NR-IQA models are all error-based attacks, where attackers aim to perturb error-based metrics like Root Mean Square Error (RMSE). Specifically, error-based attacks involve introducing imperceptible perturbations to a clean image to induce a large change in the score predicted by the NR-IQA model. The resulting perturbed image is termed an adversarial example, and the approach of manipulating input images is commonly referred to as an adversarial attack.

Perceptual attack [41] is proposed to attack available NR-IQA models. It changes predicted scores to a certain extent while maintaining the similarity between clean images and adversarial examples, incorporating human feedback in the loop. Korhonen and You [15] developed a neural network capable of generating adversarial examples, which can be used to attack unknown models. In contrast to the perceptual attack, the universal adversarial perturbation (UAP) [28] is designed to execute attacks by considering a set of images. UAP aimed at generating a universal perturbation applicable to a set of images, to collectively increase the predicted scores by an NR-IQA model. It implies the adversarial perturbation remains the same for all input images within the set. Similar to UAP, OUAP [27] also generates a universal perturbation for a set of images, maximizing the score predicted by the attacked NR-IQA model on a set of images. However, the imperceptibility of universal perturbations is not satisfactory.

It is important to note that existing methods focus on modifying the error of predicted scores without taking into account the correlation relationship between predicted scores of adversarial examples and original scores. This paper studies this aspect and offers a more comprehensive perspective to investigate the robustness of NR-IQA models.

2.2 Differential Ranking

Consider a set of image quality scores denoted as $\mathbf{s} = (s_1, s_2, \dots, s_n)$. The ranking function, defined as

$$r : \mathbf{s} \rightarrow \text{Perm}(n), \quad (1)$$

maps the set of scores to a permutation of $\{1, 2, \dots, n\}$. It evaluates at the index j to determine the position of s_j in the descending sort (a smaller rank $r_j(\mathbf{s})$ indicates a higher value for s_j). To illustrate, if $s_1 > s_3 > s_2$, then $r(\mathbf{s}) = (1, 3, 2)$. Notably, the function r is piecewise constant, rendering its derivatives either null or undefined. Consequently, this characteristic hinders the application of gradient backpropagation when we want to optimize the ranking metrics.

Many studies have explored alternative approaches to handle differentiable proxies for ranking. One feasible way is directly approximating ranking metrics, such as minimizing a smooth approximation of ranking measures through gradient descent strategies [4] or employing diverse forms of loss-augmented inference [22]. Another prevalent method is referred to as ‘‘soft’’ ranking, which can be integrated into any differential loss function. Various techniques have been employed to achieve this goal. For instance, Taylor *et al.* [35] introduced a method where each score is smoothed using equal variance Gaussian distributions. Engilberge *et al.* [8] took a different approach by training a deep neural network to learn the entire sorting operation. However, these methods tend to be time-consuming. In

contrast, Blondel *et al.* [2] proposed an efficient approach by constructing differentiable operators as projections onto the convex hull of permutations, demonstrating speed and computational friendliness. In this paper, we adopt the method proposed by Blondel *et al.* [2] during the SROCC optimization phase.

3 METHODOLOGY

In this section, Sec. 3.1 introduces the definition of correlation-error-based attacks on NR-IQA models, with a particular focus on the problem of multiple objective optimization across both correlation-based and error-based metrics. Based on this optimization problem, we propose a two-stage SROCC-MSE Attack (SMA) method, and the overall idea is illustrated in Sec. 3.2. In Sec. 3.3, we demonstrate how to get optimal target scores in Stage One. Finally, Sec. 3.4 explains how these target scores will guide the generation of adversarial examples in the targeted samples generation stage.

3.1 Problem Definition

In this paper, we consider correlation-error-based attacks on an NR-IQA model. Attackers design attack strategies based on a set of images and the goal is to perturb both the correlation relationship and score changes between predicted scores of adversarial examples and original scores of clean images. For instance, attackers may want to lead large score changes on individual images, meanwhile resulting in an inconsistency between the rankings of predicted scores and original scores.

Consider an image set $\mathcal{I} = \{I_j\}_{j=1}^N$ containing N images and $f(\cdot)$ is an NR-IQA model. The original score of image I_j predicted by $f(\cdot)$ is $s_j = f(I_j)$, and we use $\mathbf{s} := f(\mathcal{I}) = \{s_j\}_{j=1}^N$ to represent the set of original scores. Let I'_j be the perturbed version of I_j and the set of adversarial examples is denoted as $\mathcal{I}' = \{I'_j\}_{j=1}^N$. The set of predicted scores after attacks is represented as $\mathbf{s}' := f(\mathcal{I}') = \{s'_j\}_{j=1}^N$. Therefore, the optimization problem for correlation-error-based attacks is formulated as

$$\begin{aligned} \min_{\mathcal{I}'} \quad & \mathcal{L}_{\text{cor}}(f(\mathcal{I}'), f(\mathcal{I})) - \lambda \mathcal{L}_{\text{err}}(f(\mathcal{I}'), f(\mathcal{I})), \\ \text{s.t.} \quad & D(I'_j, I_j) \leq \epsilon, \forall j \in \{1, \dots, N\}. \end{aligned} \quad (2)$$

The correlation loss function, denoted as $\mathcal{L}_{\text{cor}}(\cdot, \cdot)$, is formulated based on two sets of scores, aiming to evaluate the correlation between them. The error loss function, $\mathcal{L}_{\text{err}}(\cdot, \cdot)$, is constructed for each pair of scores $\{f(I'_j), f(I_j)\}_{j=1}^N$, quantifying the prediction error between $f(I'_j)$ and $f(I_j)$. The positive λ measures the trade-off between two optimization objectives of correction and error. And $D(\cdot, \cdot)$ calculates the perceptual distance between I'_j and I_j with a pre-defined threshold ϵ . We assume that as long as I'_j and I_j satisfy the condition $D(I'_j, I_j) \leq \epsilon$, they do not appear to have a significant quality difference to human eyes so that they should have the same subjective quality perceived by humans.

In this paper, we focus on the $\mathcal{L}_{\text{cor}}(\cdot, \cdot)$ related to the ranking, and mainly consider the SROCC [33] commonly used in IQA tasks [20, 30, 31], *i.e.*,

$$\begin{aligned} \mathcal{L}_{\text{cor}}(\mathbf{s}', \mathbf{s}) &= \text{SROCC}(\mathbf{s}', \mathbf{s}) \\ &= 1 - \frac{6}{N(N^2 - 1)} \sum_{j=1}^N (r_j(\mathbf{s}') - r_j(\mathbf{s}))^2. \end{aligned} \quad (3)$$

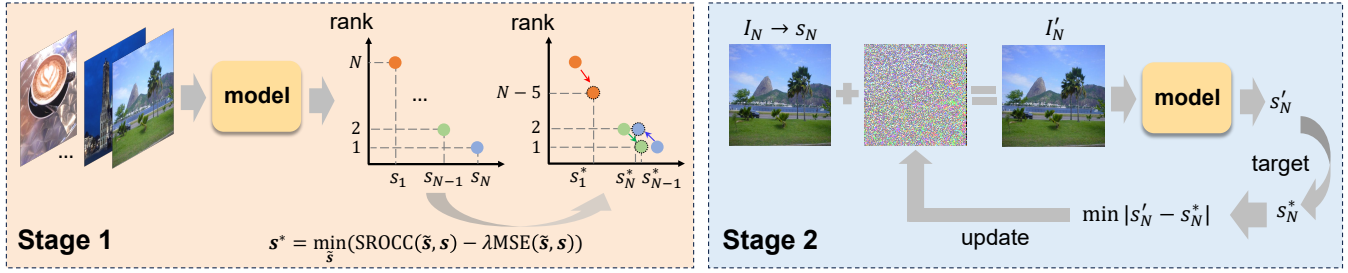


Figure 2: Overall methodology of the proposed SMA method.

Here, $r_j(\cdot)$ is the j^{th} element of the ranking function $r(\cdot)$. For $\mathcal{L}_{\text{err}}(\cdot, \cdot)$, we leverage MSE to measure the error between s'_j and s_j :

$$\mathcal{L}_{\text{err}}(s', s) = \text{MSE}(s', s) = \frac{1}{N} \sum_{j=1}^N (s'_j - s_j)^2. \quad (4)$$

The perceptual distance $D(\cdot, \cdot)$ has many choices [41], such as the ℓ_∞ norm, SSIM [36], LPIPS [40], and so on [6, 25, 26]. Among them, we choose the most commonly used ℓ_∞ norm as $D(\cdot, \cdot)$ for its simplicity in computation and optimization.

To conclude, in this paper, we aim to generate adversarial examples by solving the following optimization problem:

$$\begin{aligned} \min_{\mathcal{I}'} \quad & \text{SROCC}(f(\mathcal{I}'), f(\mathcal{I})) - \lambda_{\text{MSE}} \text{MSE}(f(\mathcal{I}'), f(\mathcal{I})), \\ \text{s.t.} \quad & \|I'_j - I_j\|_\infty \leq \epsilon, \forall j \in \{1, \dots, N\}, \end{aligned} \quad (5)$$

where $\lambda_{\text{MSE}} > 0$ is the weight to balance two attack objectives of correlation- and error-based metrics.

3.2 Overall Methodology

A straightforward approach to address the optimization problem presented in Eq. (5) is to solve it directly. However, there are two challenges. The first challenge is the storage consumption. Solving Eq. (5) directly requires the entire set \mathcal{I} to be input into $f(\cdot)$, thereby demanding gradients for every image in the set during the optimization phase. This requirement to store gradients for all images incurs considerable overhead. The second challenge is the high dimensionality of the problem defined in Eq. (5). Since the optimal solution of Eq. (5) is a set of adversarial examples, the dimensionality of this problem is $N \times d$, where d is the dimension of a single image. In many real-world applications, \mathcal{I} comprises an extensive number of large-scale images, making the direct solution of such a complex optimization problem impractical.

To overcome these challenges, we try to decompose this $N \times d$ -dimensional problem into N d -dimensional optimization problems guided by the information of $f(\mathcal{I})$. To achieve this goal, we propose a two-stage approach as illustrated in Fig. 2. In Stage One, at the score level, we find a set of target scores $\mathbf{s}^* = \{s_1^*, \dots, s_N^*\}$ which can minimize the value of $\text{SROCC}(\mathbf{s}^*, \mathbf{s}) - \lambda_{\text{MSE}} \text{MSE}(\mathbf{s}^*, \mathbf{s})$. In Stage Two, at the image level, for each image $I_j \in \mathcal{I}$, the optimization problem is to generate an adversarial example I'_j such that its predicted score is close to s_j^* as much as possible. By this two-stage approach, we decompose the original problem into two levels, score

level, and image level, which makes it easier to handle. The next two sections introduce the two stages of the proposed SMA method in detail.

3.3 Target Scores Optimization

The objective of the target scores optimization stage in SMA is to determine a set of target scores

$$\mathbf{s}^* = \arg \min_{\mathbf{s}} \text{SROCC}(\mathbf{s}, \mathbf{s}) - \lambda_{\text{MSE}} \text{MSE}(\mathbf{s}, \mathbf{s}), \quad (6)$$

where $\mathbf{s} = \{f(I_j)\}_{j=1}^N$ represents the set of original predicted scores for the image set $\mathcal{I} = \{I_j\}_{j=1}^N$, $\lambda_{\text{MSE}} > 0$ provides a trade-off between SROCC and MSE.

We find that there is a problem of \mathbf{s}^* in guiding the sample generation in Stage Two if we only minimize SROCC and maximize MSE as Eq. (6) shows. Specifically, since it is hard for Stage Two to generate adversarial examples with precisely predicted scores \mathbf{s}^* , the difference between the final predicted scores \mathbf{s}' and the target scores \mathbf{s}^* can potentially disrupt the ranking results $r(\mathbf{s}^*)$. This mismatch may result in a significant gap between the actual $\text{SROCC}(\mathbf{s}', \mathbf{s})$ and the ideal $\text{SROCC}(\mathbf{s}^*, \mathbf{s})$. For example, given three images whose original scores $\mathbf{s} = \{3, 2, 1\}$, the optimal target scores calculated in Stage One are $\mathbf{s}^* = \{4.99, 5.00, 5.01\}$, and the predicted scores of adversarial examples generated in Stage Two are $\mathbf{s}' = \{5.00, 4.99, 4.98\}$. Despite a small bias between \mathbf{s}^* and \mathbf{s}' (RMSE value is less than 0.03), the actual $\text{SROCC}(\mathbf{s}', \mathbf{s}) = 1$ significantly differs from the ideal $\text{SROCC}(\mathbf{s}^*, \mathbf{s}) = -1$.

To solve this problem, we introduce an interior-constraint strategy for target scores \mathbf{s}^* . We maximize the variance of \mathbf{s}^* so that the distribution of scores $\{s_1^*, \dots, s_N^*\}$ remains as dispersed as possible. This strategy is helpful for Stage Two, as it enhances the tolerance of bias between predicted scores and target scores. Continuing with the previous example, if target scores are $\mathbf{s}^* = \{0, 3.99, 5.01\}$, then as long as the final predicted scores \mathbf{s}' satisfy $|s'_j - s_j^*| < 0.51$, $\text{SROCC}(\mathbf{s}', \mathbf{s})$ is equivalent to $\text{SROCC}(\mathbf{s}^*, \mathbf{s})$.

Therefore, the optimization problem transforms into finding the \mathbf{s}^* that minimizes the expression:

$$\mathbf{s}^* = \arg \min_{\mathbf{s}} (\text{SROCC}(\mathbf{s}, \mathbf{s}) - \lambda_{\text{var}} \text{Var}(\mathbf{s}) - \lambda_{\text{MSE}} \text{MSE}(\mathbf{s}, \mathbf{s})), \quad (7)$$

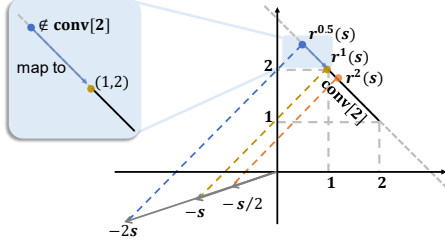


Figure 3: An example of the approximation function $r^\beta(s)$ which calculates the Euclidean projection of s/β on to $\text{conv}[N]$. In this example, $s = \{1.5, 0.5\}$ is represented by a vector $(1.5, 0.5) \in \mathbb{R}^2$.

where $\lambda_{\text{var}}, \lambda_{\text{MSE}} > 0$ represent the weight balances among the SROCC, the tolerance of bias, and the MSE. And

$$\text{Var}(\tilde{s}) = \frac{1}{N-1} \sum_{j=1}^N \left(\tilde{s}_j - \frac{1}{N} \sum_{k=1}^N \tilde{s}_k \right)^2 \quad (8)$$

is the variance of \tilde{s} .

The challenge in solving Eq. (7) arises from the non-differentiable ranking function $r(\cdot)$ when calculating $\text{SROCC}(\cdot, \cdot)$. Recall that $\text{SROCC}(\tilde{s}, s) = 1 - \frac{6}{N(N^2-1)} \sum_{j=1}^N (r_j(\tilde{s}) - r_j(s))^2$. It poses a challenge for optimizing the objective function with gradient-based algorithms due to the non-differentiability.

To solve the optimization problem defined in Eq. (7) with gradient-based methods, we approximate the non-differential ranking function $r(\cdot)$ with a differential function $r^\beta(\cdot)$ where $\beta > 0$ serves as a hyper-parameter. Following the approach of Blondel *et al.* [2], $r(\cdot)$ is approximated by

$$r^\beta(s) = \arg \min_{z \in \text{conv}[N]} \frac{1}{2} \left\| z + \frac{s}{\beta} \right\|^2, \quad (9)$$

where $\text{conv}[N]$ is a convex polytope whose vertices correspond to permutations in $[N]$. The notation $[N]$ represents all permutations of $\{1, \dots, N\}$ which contain $N!$ vertices¹. As illustrated in Fig. 3, $r^\beta(s)$ calculates the Euclidean projection of s/β on to $\text{conv}[N]$. If the projection of s/β lies outside $\text{conv}[N]$, $r^\beta(s)$ computes the nearest vertex of $\text{conv}[N]$ to the projection. The function $r^\beta(\cdot)$ is differential, as proven in the work [2]. Furthermore, the approximation error, measured by $\|r^\beta(s) - r(s)\|_2^2$, is close to zero when β is sufficiently small [2]. As a special case in [2], we have:

THEOREM 3.1. For all $s \in \mathbb{R}^N$ without ties, $r^\beta(s) = r(s)$ when

$$\beta \leq \min_{i \in \{1, \dots, N-1\}} s_{r^{-1}(i)} - s_{r^{-1}(i+1)}. \quad (10)$$

Here, $r^{-1}(\cdot)$ represents the inverse function of $r(\cdot)$, where $r^{-1}(i)$ denotes the index of the i^{th} largest element in s .

Therefore, we replace the ranking function in SROCC with $r^\beta(\cdot)$ to make the objective function differentiable. The modified objective

¹ $[N] = \{(1, 2, 3, \dots, N), (2, 1, 3, \dots, N), \dots, (N, N-1, N-2, \dots, 1)\}$.

Algorithm 1 Stage Two of SMA

Input: NR-IQA model $f(\cdot)$, original image I_j , target score s_j^* , pre-defined threshold ϵ for ℓ_∞ norm of the perturbation, iteration number m , step size α

Output: Adversarial example I'_j

- 1: Let $k \leftarrow 1, I_j^0 \leftarrow I_j$
 - 2: **while** $k \leq m$ **do**
 - 3: $\mathcal{L}_{\text{adv}} \leftarrow (f(I_j^{k-1}) - s_j^*)^2$
 - 4: $I_j^k \leftarrow I_j^{k-1} + \alpha \cdot \text{sign} \left(\nabla_{I_j^{k-1}} \mathcal{L}_{\text{adv}} \right)$
 - 5: **if** $\|I_j^k - I_j\|_\infty > \epsilon$ **then**
 - 6: Clamp pixels in I_j^k within the range $[I_j - \epsilon, I_j + \epsilon]$.
 - 7: **end if**
 - 8: $k \leftarrow k + 1$
 - 9: **end while**
 - 10: **return** $I'_j \leftarrow I_j^m$
-

function is expressed as:

$$\min_{\tilde{s}} 1 - \frac{6}{N(N^2-1)} \sum_{j=1}^N (r_j^\beta(\tilde{s}) - r_j^\beta(s))^2 - \lambda_{\text{var}} \text{Var}(\tilde{s}) - \lambda_{\text{MSE}} \text{MSE}(\tilde{s}, s). \quad (11)$$

3.4 Targeted Samples Generation

In Stage Two of SMA, for a given original image $I_j (j = 1, \dots, N)$, the objective is to generate an adversarial example I'_j with a predicted score s'_j as close to the target score s_j^* as possible. Meanwhile, I'_j is required to satisfy $\|I'_j - I_j\|_\infty \leq \epsilon$ where ϵ is a pre-defined threshold, ensuring that the adversarial perturbation remains imperceptible to human eyes. Therefore, the optimization problem for each input image is expressed as follows:

$$\min_{I'_j} (f(I'_j) - s_j^*)^2, \text{ s.t. } \|I'_j - I_j\|_\infty \leq \epsilon. \quad (12)$$

In this equation, $f(\cdot)$ represents the NR-IQA model to be attacked.

To efficiently generate I'_j satisfying Eq. (12), we draw inspiration from a classical attack method in the classification task — the fast gradient sign method (FGSM) [11]. We adopt an iterative approach to update the adversarial sample, incorporating the clamp function to ensure that $\|I'_j - I_j\|_\infty \leq \epsilon$.

In detail, we initialize the adversarial example I'_j as I_j and update I'_j iteratively using the following formula:

$$I'_j \leftarrow I'_j - \alpha \cdot \text{sign} \left(\nabla_{I'_j} (f(I'_j) - s_j^*)^2 \right), \quad (13)$$

where α is the step size, and $\text{sign}(\cdot)$ is the sign function. This update operation is repeated for m iterations. Additionally, after each update of I'_j , we clamp its pixel values to the range $[I_j - \epsilon, I_j + \epsilon]$ to satisfy the constraint condition in Eq. (12). The complete algorithm is outlined in Algorithm 1.

4 EXPERIMENTS

In this section, we present the experimental results conducted on the CLIVE [10] dataset, which collected images distorted in the wild and is challenging for the NR-IQA task. We begin by comparing the proposed SMA method with four state-of-the-art (SOTA) attack methods on four NR-IQA models in Sec. 4.1. Then we analyze the insight provided by the optimization strategy used in Stage One in Sec. 4.2. We discuss the error between the target scores and predicted scores in Stage Two in Sec. 4.3. Ablation studies that explore hyperparameters in this work are presented in Sec. 4.4.

4.1 Comparison with SOTA Attacks

We compare our method with four NR-IQA attack methods: the perceptual attack (P-attack) [41], OUAP [27], the attack method proposed by Korhonen and You (K-attack) [15], and UAP [28]. Among them, K-attack and UAP generate adversarial examples on a substitute model and then transfer these samples to the target NR-IQA model. We select four widely-used NR-IQA models as the target model: DBCNN [42], HyperIQA [34], MANIQA [38], and LIQE [43], whose architectures are based on ResNet [12], VGG [29], transformer ViT [7] and CLIP [24], respectively. For all models, 80% of the images are randomly selected from the CLIVE dataset for training NR-IQA models, with the remaining images (a total of 232 images) for testing. During the attack phase, only the test images are used. According to the original settings of these models, images with full size 500×500 are the inputs of DBCNN, and images are center-cropped to the size of 224×224 before being input to other three NR-IQA models. Additionally, we add a clipping function into the final layer of all NR-IQA models to ensure that predicted scores fall within the range of $[0, 100]$.

To comprehensively evaluate the attack performance from different perspectives, seven metrics are considered, as illustrated in Fig. 4. SROCC, KROCC, PLCC, and RMSE are conducted between predicted scores of adversarial examples and MOS provided by humans. In general, smaller values of SROCC, KROCC, and PLCC, as well as a larger value of RMSE, indicate a stronger attack. The Absolute Gain [1] calculated the MAE between the predicted score before and after the attack, which is defined as $\text{Abs.} = \frac{1}{N} \sum_{j=1}^N |f(I'_j) - f(I_j)|$, where $f(\cdot)$ is the attacked NR-IQA model, I_j and I'_j are j^{th} image and its adversarial example respectively. The R [41] is defined as:

$$R = \frac{1}{N} \sum_{j=1}^N \log \left(\frac{\max\{\beta_1 - f(I_j), f(I_j) - \beta_2\}}{|f(I_j) - f(I'_j)|} \right), \quad (14)$$

where β_1 and β_2 are the maximum MOS and minimum MOS among all MOS values. The β_1, β_2 are set to 3.50, 90.55 in our experiments. The ΔRank measures the change in the rank of each image before and after the attack, defined as:

$$\Delta\text{Rank} = \frac{1}{N} \sum_{j=1}^N |r_j(f(I')) - r_j(f(I))|, \quad (15)$$

where $r_j(f(I))$ and $r_j(f(I'))$ are the rank of the predicted score of j^{th} image before/after the attack within the image set. ΔRank provides a vital reference for the recommendation systems where the ranking of images is important. Generally, larger values of Abs., ΔRank , and a smaller value of R correspond to a stronger attack.

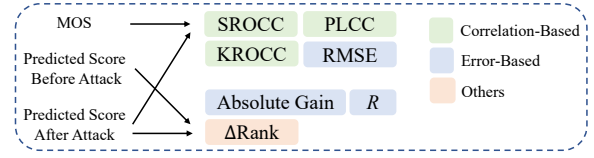


Figure 4: Evaluation metrics utilized in our experiments. Correlation-Based/ Error-Based/Other metrics are marked with different colors.

Meanwhile, we consider the imperceptibility of adversarial perturbations, ensuring that the MOS of adversarial examples is the same as that of clean images. We employ the commonly-used metrics, LPIPS [40], to quantify the visual similarity between adversarial examples and clean images. Smaller LPIPS values indicate more imperceptible perturbations.

In our experiments, we use $r^1(\cdot)$ to approximate the ranking function. $\lambda_{\text{var}}, \lambda_{\text{MSE}}$ in Eq. (11) are chosen as 0.0001 for DBCNN, HyperIQA and LIQE. For MANIQA, $\lambda_{\text{var}}, \lambda_{\text{MSE}}$ are set to 0.0002 and 0.00001, respectively. The objective in Eq. (11) is optimized 100,000 epochs with Adam optimizer [14]. The ϵ in Eq. (12) is set to 0.005. The iteration number m and step size α are set to 10, 0.005, respectively. The comparative results are shown in Table 1.

Table 1 reveals that our method consistently achieves the lowest SROCC among all compared methods while maintaining the largest RMSE values. For example, when targeting the DBCNN model, P-attack, the best-performing attack among the compared methods, achieves an SROCC of approximately -0.06 with an RMSE of nearly 54. Our method, SMA, decreases the SROCC to under -0.70 while increasing the RMSE to over 70. Notably, all compared methods exhibit their worst attack performance on MANIQA, with the SROCC values of all methods exceeding 0. Despite this, SMA still demonstrates superior performance on MANIQA, achieving an SROCC value under -0.43 , with an improvement of 0.58 over the best-performing method in our comparison.

Interestingly, despite metrics like KROCC and PLCC not being explicitly optimized in the objective function, SMA still exhibits impressive performance with the lowest KROCC, PLCC, R , and the largest Abs. values. On one hand, these results demonstrate that selecting SROCC and MSE as representative metrics for correlation-based and error-based evaluations, respectively, can also optimize other related metrics. On the other hand, it underscores the effectiveness of the proposed SMA method in attacking both error-based metrics and correlation-based metrics.

Furthermore, from the perspective of disturbing ranking, the largest ΔRank value of around 110 is achieved by SMA, which is nearly half of N . This suggests that the SMA disturbs the ranking of each image across roughly half of the entire image set on average. It further confirms the effectiveness of SMA in disturbing rankings to a great extent. More importantly, our attack results expose the vulnerability of NR-IQA to maintain ranking consistency, revealing the need for more robust NR-IQA methods in future designs.

For the invisibility of perturbations, Table 1 demonstrates that adversarial perturbations generated by our method achieve superior imperceptibility compared to most listed methods. For a more intuitive comparison, Fig. 5 provides visual results of some adversarial examples. From Fig. 5, perturbations generated by SMA and P-attack

Table 1: Comparison with SOTA methods on attacking NR-IQA models DBCNN, HyperIQA, MANIQA and LIQE (Bold/ underlined denotes the best/ the second best value in each column)

	DBCNN								HyperIQA							
	Predicted vs. MOS				Before vs. After Attack			Invis. LPIPS↓	Predicted vs. MOS				Before vs. After Attack			Invis. LPIPS↓
	SROCC↓	KROCC↓	PLCC↓	RMSE↑	Abs.↑	R ↓	ΔRank↑		SROCC↓	KROCC↓	PLCC↓	RMSE↑	Abs.↑	R ↓	ΔRank↑	
Clean	0.868	0.889	0.686	10.782	-	-	-	-	0.879	0.893	0.696	11.045	-	-	-	-
P-attack	<u>-0.061</u>	<u>-0.050</u>	<u>-0.052</u>	<u>53.960</u>	48.338	0.194	72.228	<u>0.008</u>	0.387	0.282	<u>0.218</u>	<u>39.562</u>	18.664	0.664	43.845	0.003
OUAP	0.140	0.107	0.174	46.559	25.990	0.579	70.750	0.280	<u>0.332</u>	<u>0.238</u>	<u>0.323</u>	36.990	<u>27.084</u>	<u>0.560</u>	<u>69.039</u>	0.248
K-attack	0.842	0.842	0.650	16.962	10.097	1.015	17.250	0.081	0.588	0.568	0.420	29.374	18.828	0.723	38.616	<u>0.166</u>
UAP	0.730	0.529	0.727	20.324	11.519	1.002	27.319	0.351	0.620	0.444	0.585	24.643	13.659	0.978	37.616	0.261
SMA (Ours)	-0.716	-0.570	-0.748	70.536	67.451	0.007	110.224	0.004	-0.494	-0.308	-0.648	62.204	58.268	0.083	106.302	0.003
	MANIQA								LIQE							
	Predicted vs. MOS				Before vs. After Attack			Invis. LPIPS↓	Predicted vs. MOS				Before vs. After Attack			Invis. LPIPS↓
	SROCC↓	KROCC↓	PLCC↓	RMSE↑	Abs.↑	R ↓	ΔRank↑		SROCC↓	KROCC↓	PLCC↓	RMSE↑	Abs.↑	R ↓	ΔRank↑	
Clean	0.827	0.849	0.633	27.425	-	-	-	-	0.874	0.855	0.694	18.685	-	-	-	-
P-attack	0.141	<u>0.098</u>	<u>0.046</u>	<u>44.559</u>	29.769	0.663	71.147	0.004	<u>0.195</u>	<u>0.267</u>	<u>0.137</u>	<u>45.832</u>	36.286	<u>0.730</u>	64.698	0.004
OUAP	0.182	0.128	0.236	24.717	25.629	<u>0.563</u>	68.060	0.245	0.502	0.534	0.357	28.692	25.449	0.824	47.418	0.266
K-attack	0.507	0.491	0.719	24.333	7.384	1.161	26.974	<u>0.166</u>	0.698	0.707	0.521	21.014	14.061	1.112	26.944	<u>0.166</u>
UAP	0.749	0.548	0.751	29.430	4.308	1.384	17.198	0.261	0.800	0.776	0.608	20.838	9.576	1.202	16.961	0.261
SMA (Ours)	-0.439	-0.244	-0.418	44.656	29.788	0.433	110.336	0.004	-0.526	-0.307	-0.685	66.214	75.025	0.038	112.453	0.004

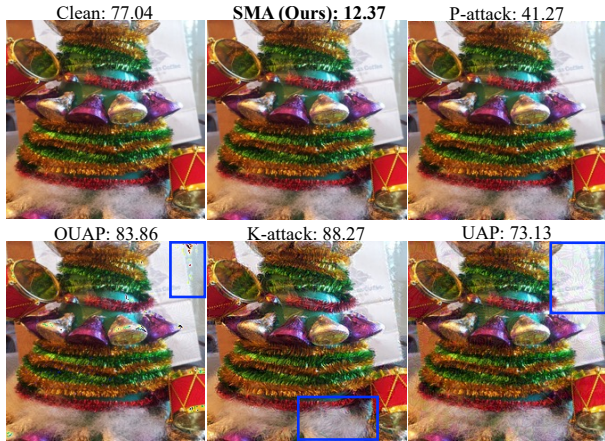


Figure 5: Visualization of adversarial examples on attacking HyperIQA. The predicted score is on the top of each image. Blue boxes indicate easily noticeable perturbations.

are imperceptible, while those introduced by OUAP, K-Attack, and UAP are easily perceivable by human observers (as shown in the blue boxes).

We also investigate the capability of SMA to manipulate predicted scores to achieve a predefined SROCC value. The experiments show the SROCC between predicted scores of images before and after the attack can approximate the predefined value with a reasonable margin of error. Such attacks may be crucial in recommendation systems where attackers aim to manipulate the score ordering of adversarial examples to follow a specific order. Besides, in addition to SROCC, the optimization of PLCC/KROCC is also explored. The optimization of PLCC generally results in successful attacks, with SMA typically yielding the best outcomes. However, for KROCC, the attack performance is less successful due to the larger differentiable approximation error resulting from the approximation of the sign function within it.

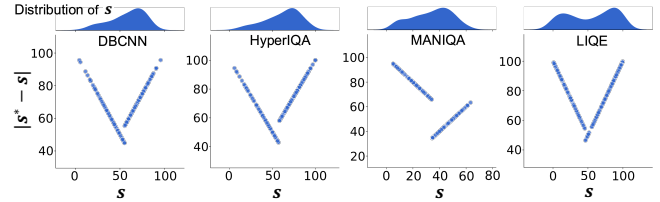


Figure 6: Relationship between original scores s and the score changes $|s^* - s|$ in Stage One.

4.2 Strategy Analysis in Stage One

In this subsection, we investigate how the optimization strategy in Stage One minimizes the value of SROCC while keeping a large prediction error between s^* and s . We calculate the score changes between target scores and original scores, *i.e.* $|s_j^* - s_j|$ for all $j \in \{1, 2, \dots, N\}$, across four NR-IQA models, and present the results in Fig. 6. Meanwhile, the density plot above illustrates the distribution of the original scores $\{s_1, s_2, \dots, s_N\}$.

From Fig. 6, it is evident that the magnitude of $|s^* - s|$ is closely related to the distribution of s . Smaller changes in scores tend to occur around the median of original scores, while larger perturbations are required for scores far from the median of original scores. This observation aligns with intuition, to maximize the change in a single score and disrupt the ranking, a large change is required far from the median to ensure that both the score and its ordering are greatly changed. It implies the optimal magnitude for each sample is related to its position relative to the median in the score set.

4.3 Error Analysis in Stage Two

In Stage One of the SMA, we compute a set of target scores with the expectation that the predicted scores of adversarial examples generated in Stage Two will be in proximity to these targets. However, the algorithm employed in Stage Two cannot guarantee exact equality between the predicted scores and target scores. Consequently, it

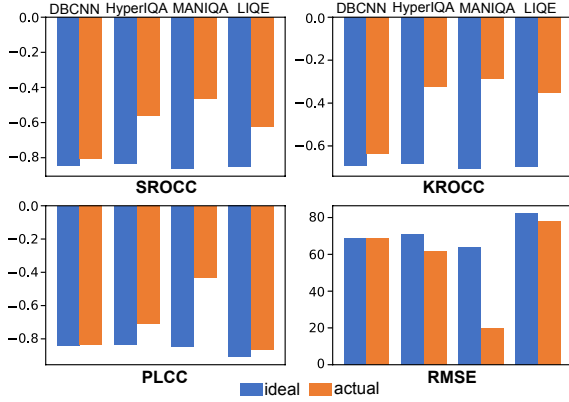


Figure 7: The comparison of ideal and actual performance in two stages. Ideal performance is assessed by comparing original scores with target scores obtained in Stage One. Actual performance is evaluated between original scores and predicted scores of adversarial examples generated in Stage Two.

becomes necessary to assess the extent of the gap between the final predicted scores and the desired target scores. To investigate this aspect, we calculate SROCC, KROCC, PLCC, and RMSE between the target scores and original scores. These results serve as the ideal performance achieved in Stage One. Simultaneously, all metrics are computed under original scores and final predicted scores, representing the actual performance obtained in Stage Two. The outcomes are illustrated in Fig. 7.

Fig. 7 reveals that the error between actual performance and ideal performance is relatively small in most cases. Take the DBCNN model as an example, the actual SROCC value is approximately -0.80 , which is only 0.04 higher than the ideal value. Similarly, the gap between ideal and actual KROCC/PLCC is less than 0.1 . Remarkably, the actual RMSE closely aligns with the ideal value. The gap of KROCC of the other three NR-IQA models is lower than 0.4 , due to the small changes in scores can easily lead to changes in pairwise comparisons. Nevertheless, the actual KROCC between predicted scores and MOS is still far better than the other attacked methods in Table 1. MANIQA is an exception whose actual RMSE is significantly worse than the ideal one. We attribute this phenomenon to the robustness of MANIQA. Even though the target scores for many samples are close to 0 , the predicted scores fall within a narrow range of $[5, 60]$. This discrepancy results in a significant gap between the target and actual predicted scores.

4.4 Ablation Study

There are three main hyperparameters in SMA: β in the approximation function $r^\beta(\cdot)$, the multiplier λ_{var} , and λ_{MSE} in Eq. (11). We present ablation studies on them with the target model HyperIQA.

Approximation function $r^\beta(\cdot)$. According to Theorem 3.1, a small value of β is preferable for approximation. However, a small β also results to sparse gradients of $r^\beta(\tilde{s})$ with respect to \tilde{s} , making it challenging to optimize $\text{SROCC}(\tilde{s}, s)$ and $\text{MSE}(\tilde{s}, s)$. Experimental results in Table 2 support this point. We explore various β through 100,000 optimization steps in Stage One. We then present metrics $\text{SROCC}^\beta(s^*, s) = 1 - \frac{6}{N(N^2-1)} \sum_{j=1}^N \left(r_j^\beta(s^*) - r_j(s) \right)^2$ and

Table 2: Ablation study of β in the approximation function $r^\beta(\cdot)$

β	0.2	0.4	0.6	0.8	1.0
SROCC^β	0.5035	-0.7691	-0.8655	-0.8301	-0.8316
RMSE	27.7607	48.6960	70.1683	70.9954	71.0056
error	0.0166	0.0461	0.0605	0.0669	0.0673

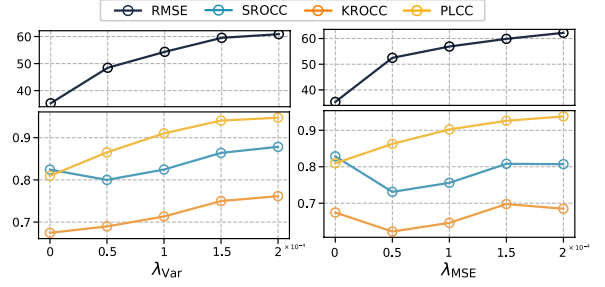


Figure 8: Ablation studies of the multiplier λ_{var} and λ_{MSE} .

$\text{RMSE}(s^*, s)$ to assess the optimization efficiency. A smaller SROCC^β and a larger RMSE indicate faster optimization of SROCC and MSE, respectively. We also quantify the approximation error as $|\text{SROCC}^\beta(s^*, s) - \text{SROCC}(s^*, s)|$. From Table 2, as β increases, the optimization of the objective in Eq. (11) becomes more manageable, resulting in a smaller $\text{SROCC}^\beta(s^*, s)$ and a greater $\text{RMSE}(s^*, s)$, while the error also generally grows. Nonetheless, the maximum error remains under 0.1 , which is considered acceptable.

The weight λ_{var} in Eq. (11). A larger λ_{var} implies a stricter constraint on the target score variance, making the target easier to achieve in Stage Two. This can be measured by the consistency between the target scores s^* and actual predicted scores $f(I')$. Fig. 8 (left) confirms this point by illustrating the effect of λ_{var} when $\lambda_{\text{MSE}} = 0$. In Fig. 8, the correlations are calculated between s^* and $f(I')$, and the RMSE is calculated between s and $f(I')$. With the increase of λ_{var} , the correlation between s^* and $f(I')$ generally increased. It confirms the effectiveness of $\text{Var}(\cdot)$ in improving the consistency between target scores and actual predicted scores.

The weight λ_{MSE} in Eq. (11). A larger λ_{MSE} implies a more strict constraint on the error between target scores and original scores, thereby enhancing the error between original scores and predicted scores of adversarial examples generated in Stage Two. Fig. 8 (right) illustrates the impact of λ_{MSE} when $\lambda_{\text{var}} = 0$. As λ_{MSE} increases, the RMSE between s and $f(I')$ also increases, confirming the effectiveness of $\text{MSE}(\cdot, \cdot)$ in boosting the error between predicted scores before and after the attack. Meanwhile, the increase of λ_{MSE} will decrease SROCC to some extent.

5 CONCLUSION

This paper introduces a novel framework of correlation-error-based adversarial attacks on NR-IQA models. We present a two-stage method, SMA, which disrupts both individual image scores and intra-set correlations with excellent performance. It highlights NR-IQA's vulnerability in preserving scores and correlations. SMA provides a thorough assessment of robustness in NR-IQA, laying the groundwork for future research on more robust NR-IQA models.

REFERENCES

- [1] Anastasia Antsiferova, Khaled Abud, Aleksandr Gushchin, Ekaterina Shumitskaya, Sergey Lavrushkin, and Dmitriy Vatolin. 2024. Comparing the robustness of modern no-reference image- and video-quality metrics to adversarial attacks. In *AAAI Conference on Artificial Intelligence*. 700–708.
- [2] Mathieu Blondel, Olivier Teboul, Quentin Berthet, and Josip Djolonga. 2020. Fast Differentiable Sorting and Ranking. In *ICML*. 950–959.
- [3] Sebastian Bosse, Dominique Maniry, Klaus-Robert Müller, Thomas Wiegand, and Wojciech Samek. 2018. Deep Neural Networks for No-Reference and Full-Reference Image Quality Assessment. *IEEE Transactions on Image Processing* 27, 1 (2018), 206–219.
- [4] Olivier Chapelle and Mingrui Wu. 2010. Gradient descent optimization of smoothed information retrieval metrics. *Information Retrieval* 13, 3 (2010), 216–235.
- [5] Ziwen Chen, Kaushik Patnaik, Shuangfei Zhai, Alvin Wan, Zhile Ren, Alexander G. Schwing, Alex Colburn, and Fuxin Li. 2023. AutoFocusFormer: Image Segmentation off the Grid. In *IEEE/CVF Conference on Computer Vision and Pattern Recognition*. 18227–18236.
- [6] Keyan Ding, Kede Ma, Shiqi Wang, and Eero P. Simoncelli. 2022. Image quality assessment: Unifying structure and texture similarity. *IEEE Transactions on Pattern Analysis and Machine Intelligence* 44, 5 (2022), 2567–2581.
- [7] Alexey Dosovitskiy, Lucas Beyer, Alexander Kolesnikov, Dirk Weissenborn, Xiuhua Zhai, Thomas Unterthiner, Mostafa Dehghani, Matthias Minderer, Georg Heigold, Sylvain Gelly, Jakob Uszkoreit, and Neil Houlsby. 2021. An image is worth 16 × 16 words: Transformers for image recognition at scale. In *International Conference on Learning Representations*. 1–21.
- [8] Martin Engilberge, Louis Chevallier, Patrick Pérez, and Matthieu Cord. 2019. SoDeep: A Sorting Deep Net to Learn Ranking Loss Surrogates. In *IEEE/CVF Conference on Computer Vision and Pattern Recognition*. 10792–10801.
- [9] Ruopeng Gao and Limin Wang. 2023. MeMOTR: Long-Term Memory-Augmented Transformer for Multi-Object Tracking. In *IEEE/CVF Conference on Computer Vision and Pattern Recognition*. 9901–9910.
- [10] Deepti Ghadiyaram and Alan C. Bovik. 2016. Massive Online Crowdsourced Study of Subjective and Objective Picture Quality. *IEEE Transactions on Image Processing* 25, 1 (2016), 372–387.
- [11] Ian J. Goodfellow, Jonathon Shlens, and Christian Szegedy. 2015. Explaining and harnessing adversarial examples. In *International Conference on Learning Representations*. 1–11.
- [12] Kaiming He, Xiangyu Zhang, Shaoqing Ren, and Jian Sun. 2016. Deep residual learning for image recognition. In *IEEE/CVF Conference on Computer Vision and Pattern Recognition*. 770–778.
- [13] Maurice G. Kendall. 1938. A New Measure of Rank Correlation. *Biometrika* 30, 1/2 (1938), 81–93. <http://www.jstor.org/stable/2332226>
- [14] Diederik P. Kingma and Jimmy Ba. 2015. Adam: A Method for Stochastic Optimization. In *International Conference on Learning Representations*. 1–15.
- [15] Jari Korhonen and Junyong You. 2022. Adversarial Attacks Against Blind Image Quality Assessment Models. In *Proceedings of the 2nd Workshop on Quality of Experience in Visual Multimedia Applications*. 3–11.
- [16] Dingquan Li, Tingting Jiang, and Ming Jiang. 2020. Norm-in-Norm Loss with Faster Convergence and Better Performance for Image Quality Assessment. In *ACM International Conference on Multimedia*. 789–797.
- [17] Siyuan Li, Xing Xu, Zailai Zhou, Yang Yang, Guoqing Wang, and Heng Tao Shen. 2022. ARRA: Absolute-Relative Ranking Attack against Image Retrieval. In *ACM International Conference on Multimedia*. 610–618.
- [18] Yang Li, Shiqi Wang, Xinfeng Zhang, Shanshe Wang, Siwei Ma, and Yue Wang. 2021. Quality Assessment of End-to-End Learned Image Compression: The Benchmark and Objective Measure. In *ACM International Conference on Multimedia*. 4297–4305.
- [19] Xiaoyu Ma, Chenxi Feng, Jiaojiao Wang, Qiang Lin, Suiyu Zhang, Jinchi Zhu, Xiaodiao Chen, Chang Liu, and Dingguo Yu. 2023. A Model-Agnostic Semantic-Quality Compatible Framework based on Self-Supervised Semantic Decoupling. In *ACM International Conference on Multimedia*. 6774–6784.
- [20] Pavan C. Madhusudana, Neil Birkbeck, Yilin Wang, Balu Adsumilli, and Alan C. Bovik. 2022. Image quality assessment using contrastive learning. *IEEE Transactions on Image Processing* 31 (2022), 4149–4161.
- [21] Hanene F.Z.B. Meftah, Sid A. Fezza, Wassim Hamidouche, and Olivier Déforges. 2023. Evaluating the Vulnerability of Deep Learning-based Image Quality Assessment Methods to Adversarial Attacks. In *European Workshop on Visual Information Processing*. 1–6.
- [22] Pritish Mohapatra, Michal Rolínek, C. V. Jawahar, Vladimir Kolmogorov, and M. Pawan Kumar. 2018. Efficient Optimization for Rank-Based Loss Functions. In *IEEE/CVF Conference on Computer Vision and Pattern Recognition*. 3693–3701.
- [23] Karl Pearson. 1895. Note on Regression and Inheritance in the Case of Two Parents. *Proceedings of the Royal Society of London* 58 (1895), 240–242.
- [24] Alec Radford, Jong Wook Kim, Chris Hallacy, Aditya Ramesh, Gabriel Goh, Sandhini Agarwal, Girish Sastry, Amanda Askell, Pamela Mishkin, Jack Clark, Gretchen Krueger, and Ilya Sutskever. 2021. Learning transferable visual models from natural language supervision. In *ICML*. 8748–8763.
- [25] Rafael Reisenhofer, Sebastian Bosse, Gitta Kutyniok, and Thomas Wiegand. 2018. A Haar wavelet-based perceptual similarity index for image quality assessment. *Signal Processing: Image Communication* 61 (2018), 33–43.
- [26] Hamid R Sheikh and Alan C Bovik. 2006. Image information and visual quality. *IEEE Transactions on Image Processing* 15, 2 (2006), 430–444.
- [27] Ekaterina Shumitskaya, Anastasia Antsiferova, and Dmitriy Vatolin. 2024. Towards adversarial robustness verification of no-reference image- and video-quality metrics. *Computer Vision and Image Understanding* 240 (2024), 103913.
- [28] Ekaterina Shumitskaya, Anastasia Antsiferova, and Dmitriy S. Vatolin. 2022. Universal Perturbation Attack on Differentiable No-Reference Image- and Video-Quality Metrics. In *British Machine Vision Conference*. 1–12.
- [29] Karen Simonyan and Andrew Zisserman. 2015. Very Deep Convolutional Networks for Large-Scale Image Recognition. In *International Conference on Learning Representations*. 1–14.
- [30] Maksim Siniukov, Dmitriy Kulikov, and Dmitriy Vatolin. 2022. Applicability limitations of differentiable full-reference image-quality metrics. *arXiv preprint arXiv:2212.05499* (2022).
- [31] Maksim Siniukov, Dmitriy Kulikov, and Dmitriy Vatolin. 2023. Unveiling the Limitations of Novel Image Quality Metrics. In *IEEE International Workshop on Multimedia Signal Processing*. 1–6.
- [32] Biju Venkadath Somasundaran, Rajiv Soundararajan, and Soma Biswas. 2020. Robust image retrieval by cascading a deep quality assessment network. *Signal Processing: Image Communication* 80 (2020), 115652.
- [33] Charles Spearman. 1961. The proof and measurement of association between two things. *The American Journal of Psychology* 16, 1 (1961), 72–101. <https://doi.org/10.2307/1412159>
- [34] Shaolin Su, Qingsen Yan, Yu Zhu, Cheng Zhang, Xin Ge, Jinqiu Sun, and Yanning Zhang. 2020. Blindly Assess Image Quality in the Wild Guided by a Self-Adaptive Hyper Network. In *IEEE/CVF Conference on Computer Vision and Pattern Recognition*. 3664–3673.
- [35] Michael Taylor, John Guiver, Stephen Robertson, and Tom Minka. 2008. Soft-Rank: optimizing non-smooth rank metrics. In *Proceedings of the International Conference on Web Search and Data Mining*. 77–86.
- [36] Zhou Wang, Alan C. Bovik, Hamid R. Sheikh, and Eero P. Simoncelli. 2004. Image quality assessment: From error visibility to structural similarity. *IEEE Transactions on Image Processing* 13, 4 (2004), 600–12.
- [37] Chenxi Yang, Yujia Liu, Dingquan Li, and Tingting Jiang. 2024. Exploring Vulnerabilities of No-Reference Image Quality Assessment Models: A Query-Based Black-Box Method. *arXiv preprint arXiv:2401.05217* (2024).
- [38] Sidi Yang, Tianhe Wu, Shuwei Shi, Shanshan Lao, Yuan Gong, Mingdeng Cao, Jiahao Wang, and Yujia Yang. 2022. MANIQA: Multi-dimension Attention Network for No-Reference Image Quality Assessment. In *IEEE/CVF Conference on Computer Vision and Pattern Recognition Workshops*. 1190–1199.
- [39] Ao-Xiang Zhang, Yu Ran, Weixuan Tang, and Yuan-Gen Wang. 2023. Vulnerabilities in Video Quality Assessment Models: The Challenge of Adversarial Attacks. In *Advances in Neural Information Processing Systems*. 1–14.
- [40] Richard Zhang, Phillip Isola, Alexei A. Efros, Eli Shechtman, and Oliver Wang. 2018. The Unreasonable Effectiveness of Deep Features as a Perceptual Metric. In *IEEE/CVF Conference on Computer Vision and Pattern Recognition*. 586–595.
- [41] Weixia Zhang, Dingquan Li, Xiongkuo Min, Guangtao Zhai, Guodong Guo, Xiaokang Yang, and Kede Ma. 2022. Perceptual Attacks of No-Reference Image Quality Models with Human-in-the-Loop. In *Advances in Neural Information Processing Systems*. 2916–2929.
- [42] Weixia Zhang, Kede Ma, Jia Yan, Dexiang Deng, and Zhou Wang. 2020. Blind Image Quality Assessment Using a Deep Bilinear Convolutional Neural Network. *IEEE Transactions on Circuits and Systems for Video Technology* 30, 1 (2020), 36–47.
- [43] Weixia Zhang, Guangtao Zhai, Ying Wei, Xiaokang Yang, and Kede Ma. 2023. Blind Image Quality Assessment via Vision-Language Correspondence: A Multitask Learning Perspective. In *IEEE/CVF Conference on Computer Vision and Pattern Recognition*. 14071–14081.
- [44] Wei Zhou and Zhou Wang. 2022. Quality Assessment of Image Super-Resolution: Balancing Deterministic and Statistical Fidelity. In *ACM International Conference on Multimedia*. 934–942.